

Original Research Article

Synthesis and Characterization of PEDOT: PSS-PA with good electrical conductivity for supercapacitor

Abstract

Recently, researches on molecular engineering of PEDOT:PSS is being actively conducted to improve the electrical conductivity and device performance. In this paper, we prepared and characterized a series of PSS substituted with alkyl sulfonate (PSS-co-PA3, PSS-co-PA5, PSS-co-PA10, and PSS-co-PA30) proceeding to prepare additive-free PEDOT:PSS/graphene oxide (GO) aerogels with different amounts of alkyl sulfonate functional groups that could be applied to supercapacitor electrodes. The introduction of alkyl sulfonate groups in PSS can enhance its solubility due to the flexible alkyl sulfonate groups. The cycle stability of supercapacitors using PEDOT:PSS-co-PAs/rGO composites was improved compared with its devices using of Clevios4083/rGO.

Keywords: Conducting polymers, PEDOT:PSS, graphene oxide, supercapacitor, electrical conductivity

Introduction

With the continuous progress and development of human beings, energy storage remains an important issue for us because of its required constant fossil depletion and global climate change. In particular, the main electrical energy storage systems include fuel cells, batteries, and supercapacitors.[1-4] Among them, supercapacitors have a greater potential for applications than batteries and fuel cells due to their high power density, fast charging and

discharging, long cycle life, and low energy density.[3] An important factor in the fabrication of efficient supercapacitors is electrodes with high capacitance and high conductivity, and the electrode materials that have received much attention are carbon materials, metal oxides, conducting polymers and their composites.[5-8]

Poly(3,4-ethylenedioxythiophene):poly(styrene sulfonate sodium) (PEDOT:PSS), which is the most successful conductive polymer commercially named as Clevios 4083, has been widely used as an electrode in supercapacitors due to its many outstanding properties including excellent electrical conductivity, good film-forming ability, large pseudo-capacitance, fast charging-discharging processes, wide voltage range, electrochemical reversibility, and high mechanical adaptability.[7] However, PEDOT:PSS also exhibited a poor electrochemical activity and short cycle life because of the insulating and hygroscopic nature of PSS. To address these issues, the combination of carbon materials and PEDOT:PSS has attracted the attention of a wide range of researchers.[9-12]

In comparison with other carbon materials, graphene and its derivatives have emerged as the most potential electrode materials for supercapacitors owing to their large surface area, excellent electrical conductivity and mechanical properties.[10] Therefore, a large number of graphene-based composites, such as PEDOT:PSS/reduced graphene oxide (rGO) composites, are the most promising candidates for good electrochemical performance of electrodes though the synergistic effect. However, these composite electrodes of supercapacitors still have a poor cycle life attributed to the hygroscopic and insulating nature of PSS. Many approaches have been proposed to improve the electrical conductivity and stability of PEDOT:PSS, such as the addition additives, heat treatment, etc.[13] Among them, the introduction of acrylic acid into the PSS chain as a dopant for PEDOT, and its films have shown better stability, water resistance, and more flexibility. Interestingly, the introduction of

acrylic acid into PEDOT:PSS did not lead to a decrease in conductivity owing to its anionic group which also provided doping performance for the synthesis of PEDOT.[14] Recently, Yano et al. prepared alkyl sulfonate-substituted PEDOT and studied the effect of molecular weight of PEDOT on their electrical conductivity. Alkyl sulfonate-substituted PEDOT can be dissolved in various organic solvent and water due to the flexible alkyl sulfonate groups. The molecular weight of PEDOT was a key factor in improving electrical conductivity.[15] More recently, Yeon et al. enhanced device performance and electrical stability of PEDOT:PSS by the blended alkyl sulfonate surfactants, which changed the conformational of PEDOT chains.[16] However, the polymerization of bulky substituted EDOT monomers or the use of additive methods without phase separation to obtain the desired devices is still challenging.

In this paper, we prepared and characterized a series of PSS substituted with alkyl sulfonate (PSS-co-PA3, PSS-co-PA5, PSS-co-PA10, PSS-co-PA30, and PSS-b-PA30), poly(styrene sulfonate-co-sulfopropyl acrylate)s, poly(styrene sulfonate-b-sulfopropyl acrylate), proceeding to prepare additive-free PEDOT:PSS/rGO aerogels with different amounts of alkyl sulfonate functional groups that could be applied to supercapacitor electrodes. The cycle stability of supercapacitors using PEDOT:PSS-co-PAs/rGO composites was improved compared with its devices using of Clevios 4083/rGO.

Experimental Section

Materials

Chemicals such as sodium-4-vinylbenzenesulfonate (NaSS), potassium persulfate ($K_2S_2O_8$), sodium bisulfite ($NaHSO_3$), sodium persulfate ($Na_2S_2O_8$), 3-sulfopropyl acrylate potassium salt (SPAK), Hydrochloric acid (HCl), 4,4'-azobis(4-cyanovaleric acid) (ACVA), 3,4-ethylenedioxythiophene (EDOT), 4-cyano-4-(phenylcarbonothioylthio) pentanoic acid,

ferrous sulfate heptahydrate ($\text{FeSO}_4 \cdot 7\text{H}_2\text{O}$) were purchased from Aldrich used without any further purification. Clevios 4083 and rGO was purchased from Heraeus. The ion exchange resin was purchased from Samyang Co. All other chemical solvents were purchased from Aldrich and purified by distillation before use.

Synthesis of PSS-co-PA3 A solution of sodium-4-vinylbenzenesulfonate (3.39g, 16.44 mmol) and 3-sulfopropyl acrylate potassium salt (0.12g, 0.52 mmol) in distilled water (20 mL) were mixed for 10 minutes. The powder of $\text{K}_2\text{S}_2\text{O}_8$ (1.78 wt% per monomer) and NaHSO_3 (0.86 wt% per monomer) was added into the solution. The reaction mixture was heated to 45°C in a water bath and stirred at for 7 h under an N_2 atmosphere. The solution was dialyzed using a semi-permeable membrane after cooling to room temperature. Dialysate was changed by fresh distilled water hourly until the conductivity of the dialysate was similar to that of distilled water. The PSS-co-PA3 product was obtained by mixing the equal volume of cationic ion exchange resin and stirring at 30°C for 2 h. Consequently, the dialyzed solution was evaporated and dried in a vacuum oven to give PSS-co-PA3 (2.3 g, 66 % yield). ^1H NMR (400 MHz, D_2O , δ , ppm): 8.0-6.0 (aromatic-CH), 2.5 ($\text{CH}_2\text{-SO}_3^-$), 1.0-1.6 (CH- CH_2). FT-IR (cm^{-1}): 1140-1250 (O=S=O), 1725 (O=C-O), 1412-1495 (C=C). aqueous GPC: $M_n=17$ kDa, $M_w=55$ kDa, PDI= 3.2.

Synthesis of PSS-co-PA5 Following the similar procedure of the compound PSS-co-PA3 using different ratios of NaSS (3.31 g, 16.05 mmol) and SPAK (0.2 g, 0.86 mmol). (2.6 g, 74 % yield). ^1H NMR (400 MHz, D_2O , δ , ppm): 8.0-6.0 (aromatic-CH), 2.5 ($\text{CH}_2\text{-SO}_3^-$), 1.0-1.6 (CH- CH_2). FT-IR (cm^{-1}): 1140-1250 (O=S=O), 1725 (O=C-O), 1412-1495 (C=C). aqueous GPC: $M_n=22$ kDa, $M_w=74$ kDa, PDI= 3.4.

Synthesis of PSS-co-PA10 Following the similar procedure of the compound PSS-co-PA3 using different ratios of NaSS (3.11 g, 15.08 mmol) and SPAK (0.4 g, 1.72 mmol). (2.42 g,

69 % yield). $^1\text{H NMR}$ (400 MHz, D_2O , δ , ppm): 8.0-6.0 (aromatic-CH), 2.5 ($\text{CH}_2\text{-SO}_3^-$), 1.0-1.6 (CH-CH_2). FT-IR (cm^{-1}): 1140-1250 (O=S=O), 1725 (O=C-O), 1412-1495 (C=C). aqueous GPC: $M_n=30$ kDa, $M_w=97$ kDa, $\text{PDI}=3.2$.

Synthesis of PSS-co-PA30 Following the similar procedure of the compound PSS-co-PA3 using different ratios of NaSS (2.31 g, 11.2 mmol) and SPAK (1.2 g, 5.17 mmol). (2.9 g, 83 % yield). $^1\text{H NMR}$ (400 MHz, D_2O , δ , ppm): 8.0-6.0 (aromatic-CH), 2.5 ($\text{CH}_2\text{-SO}_3^-$), 1.0-1.6 (CH-CH_2). FT-IR (cm^{-1}): 1140-1250 (O=S=O), 1725 (O=C-O), 1412-1495 (C=C). aqueous GPC: $M_n=34$ kDa, $M_w=88$ kDa, $\text{PDI}=2.6$.

Synthesis of macro-PSS In a mixture of water (19 mL) and ethanol (7 mL), NaSS (6.12 g, 29.7 mmol) 4-cyano-4-(phenylcarbonothioylthio)pentanoic acid (55 mg, 0.2 mmol), and ACVA (22.4 mg, 0.08 mmol) were mixed. Then, the mixture was degassed with nitrogen for 30 minutes. After being set in an oil bath at 70°C , the reaction mixture was allowed to run its course for 16 hours. Exposure to air stopped the reaction. The solution was purified by precipitation in acetone and dried under vacuum to afford macro-PSS. (5.5 g, 90% yield). $^1\text{H NMR}$ (400 MHz, D_2O , δ , ppm): 8.0-6.0 (aromatic-CH), 1.0-1.6 (CH-CH_2). FT-IR (cm^{-1}): 1140-1250 (O=S=O), 1412-1495 (C=C). aqueous GPC: $M_n=20.9$ kDa, $M_w=47.8$ kDa, $\text{PDI}=2.3$.

Synthesis of PSS-b-PA30 SPAK (0.25g, 1.08 mmol), ACVA (7 mg, 0.03 mmol), and PSS (0.53 g, 2.57 mmol) were dissolved in 10 mL of water and allowed to degas for 30 minutes while under a nitrogen flow. The mixture was heated to 70°C for 16 h in an oil bath. Rapidly cool on dry ice and expose to air to stop the reaction. The solution was purified by precipitation in acetone and dried under vacuum to give PSS-b-PA30 as a pink powder. (0.75 g, 96% yield). $^1\text{H NMR}$ (400 MHz, D_2O , δ , ppm): 8.0-6.0 (aromatic-CH), 4.1 (O-CH_2), 2.9

(CH₂-SO₃⁻), 1.95 (CH₂), 1.0-1.6 (CH-CH₂). FT-IR (cm⁻¹): 1140-1250 (O=S=O), 1725 (O=C-O), 1412-1495 (C=C). aqueous GPC: Mn=24.9 kDa, Mw=50.5 kDa, PDI=2.0.

Synthesis of PEDOT:PSS-PAs composites The PEDOT:PSS-PAs composites were synthesized by oxidative polymerization. The copolymers (PSS-co-PA3, PSS-co-PA5, PSS-co-PA10, PSS-co-PA30 and PSS-b-PA30) (0.38 g) in distilled water (20 mL) was mixed with sodium persulfate (0.18 g, 0.98 wt%) and ferrous sulfate heptahydrate (0.04 g, 0.2 wt%). 3,4-Ethylenedioxythiophene (EDOT) monomers (0.07 mL, 0.5 wt%) were added to the mixture. The reaction mixture was stirred at 20 °C for 24 h. The mixture was removed sodium and sulfate ions by mixing with cation and anion exchange resins for 24 h and filtering with 30 µm mesh filter. Then, the semi-permeable membrane was used to dialyze the solution against distilled water until the conductivity of dialysate was the same as that of distilled water. After the dialysis, five different solutions were prepared as referred PEDOT:PSS-co-PA3, PEDOT:PSS-co-PA5, PEDOT:PSS-co-PA10, PEDOT:PSS-co-PA30 and PEDOT:PSS-b-PA30. FT-IR (cm⁻¹): 1624 (C=C), 1523 (C-C), 1388 (C-O-C), 1140-1250 (O=S=O), 1412-1495 (C=C).

Preparation of porous PEDOT:PSS-co-PA30/rGO aerogel PEDOT:PSS-co-PA30/rGO aerogel was prepared through the hydrothermal reaction. rGO (75 mg) was added to distilled water (30 mL) and dispersed by sonication in order to form a uniform rGO dispersion. 1.5 wt% PEDOT:PSS-co-PA30 solution (1 mL) was mixed into rGO dispersion for 6 hours. Then, the mixture was put into a 70 ml Teflon-lined autoclave and heated at 180 °C for 2 h to make a cylindrical hydrogel. The PEDOT:PSS-co-PA30/rGO composite aerogel was obtained by freeze-drying process.

Preparation of porous PEDOT:PSS-b-PA30/rGO aerogel Following the similar procedure of the PEDOT:PSS-co-PA30/rGO aerogel.

Characterization ^1H NMR (Bruker Biospin, Avance III HD, 400 MHz), FT-IR (Bruker, Vortex 70), UV-vis spectrometer (Shimadzu UV-3600) were used to characterize the structure of the copolymers. For measuring the molecular weights of the copolymers, gel permeation chromatography (GPC) (ACME9000 equipped with a series of Water columns; Ultrahydrogel 120, 250, 500, 2000) was utilized. The elemental compositions and ratio of PEDOT to PSS were analyzed by X-ray photoelectron spectroscopy (XPS, Thermo Fisher Scientific, K-Alpha+). The topography images of the films for PEDOT:PSS-PAs were taken with atomic force microscope (AFM, Surface imaging systems-GmbH, Picostation). The sheet resistance was tested on a four-point measuring device. Field emission scanning electron microscopy (FESEM, NOVA NanoSEM450) was used to analyze the morphology and structure of the aerogels.

Electrochemical measurements A piece of aerogel was pressed into a circular sheet to manufacture the working electrode. Cyclic voltammograms (CV), galvanostatic charge-discharge (GCD), and electrochemical impedance spectroscopy (EIS) measurements were performed on a potentiostat (VSP-300, Biologic Science Instruments) with aqueous 1M H_2SO_4 solution as the electrolyte. The specific capacitance (C), power density (P), and energy density (E), were evaluated according to the following formulas:

$$C = \frac{I\Delta t}{m\Delta V} \quad (1)$$

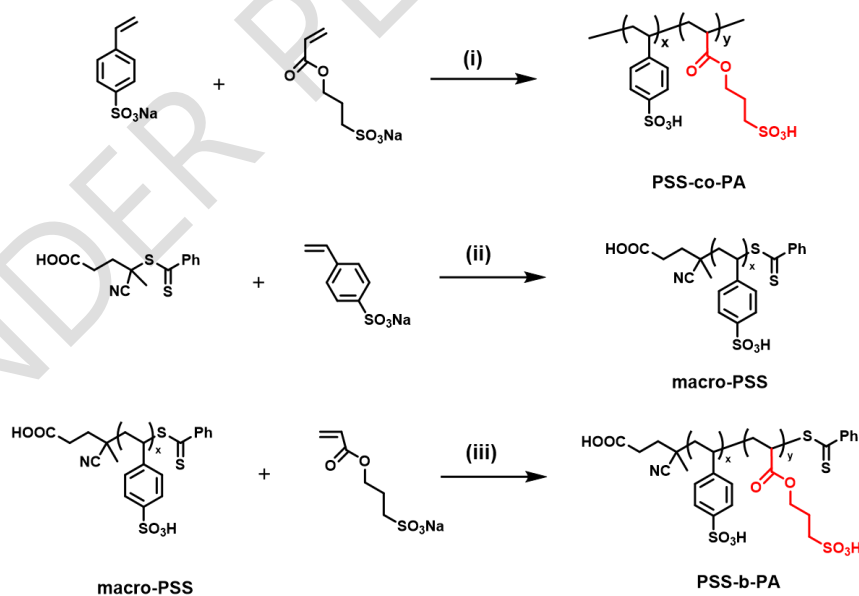
$$E = \frac{C_{\text{cell}} \Delta V^2}{2 \times 3.6} \quad (2)$$

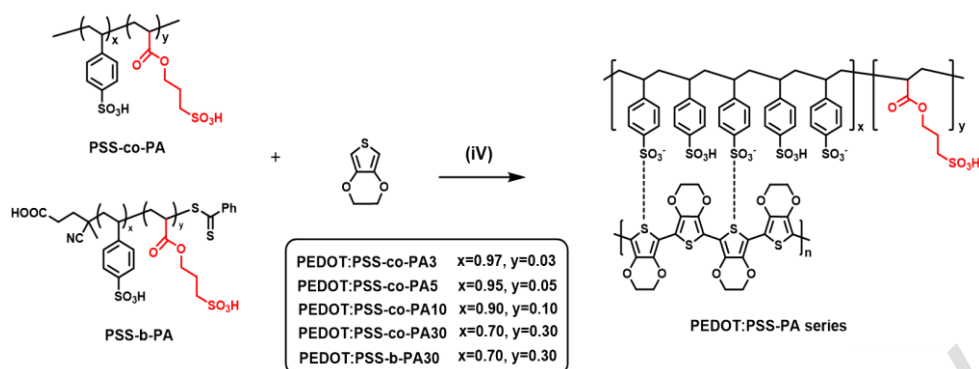
$$P = \frac{3600E}{\Delta t} \quad (3)$$

where I represents the discharge current (A), Δt the discharge time (s), m the mass of electrode (g), Δv potential window (V), C the gravimetric specific capacitance of the electrode, and C_{cell} the gravimetric specific capacitance of the supercapacitor.

Results and Discussion

Alkyl sulfonate functional groups were incorporated into the PSS main chains to obtain the random and block copolymers of PSS-PA series (PSS-co-PA3, PSS-co-PA5, PSS-co-PA10, PSS-co-PA30 and PSS-b-PA30). The random copolymers were synthesized by free radical polymerization using potassium persulfate ($\text{K}_2\text{S}_2\text{O}_8$) as the initiator (**Scheme 1**). The block copolymers were prepared by reversible addition-fragmentation chain-transfer polymerization (RAFT) using 4,4'-azobis(4-cyanovaleric acid) (ACVA) as the initiator. In particular, PSS-co-PA30 and PSS-b-PA30 have a high yield and high molecular weight.





Scheme 1. Synthetic routes to copolymers and PEDOT:PSS-PA series complexes. (i) NaSO_3 , $\text{K}_2\text{S}_2\text{O}_8$; (ii) ACVA, H_2O ; (iii) ACVA, H_2O ; (iv) $\text{Na}_2\text{S}_2\text{O}_8$, $\text{FeSO}_4 \cdot 7\text{H}_2\text{O}$.

The ^1H NMR and FT-IR spectra of the copolymers were used to analyze the structure and the molar ratio of the introduced alkyl sulfonate functional groups. In the ^1H NMR spectrum of the PSS-PA series copolymers (**Figure 1**), the four protons of the aromatic ring were relevant for the peaks at 7.5 and 6.8 ppm, while the six protons on the side chain of the alkyl sulfonate functional groups were responsible for the peaks at 4.1, 2.9, and 1.95 ppm. However, we have found that the ^1H NMR spectrum of the random copolymers (PSS-co-PAs) appeared only two protons on the side of the sulfonic acid group on the alkyl sulfonate functional groups. This might be explained by the space barrier between PSS-co-PAs molecules. The integration area of 6.8 and 2.9 ppm can be used to determine the proportion of alkyl sulfonate groups in the main backbone chains. For PSS-co-PA3, PSS-co-PA5, PSS-co-PA10, PSS-co-PA30 and PSS-b-PA30, the percentages of alkyl sulfonate groups in the main backbone chains were almost 3, 5, 10, 30 and 30, respectively, which were almost the same as the feed ratios of NaSS and SPAK.

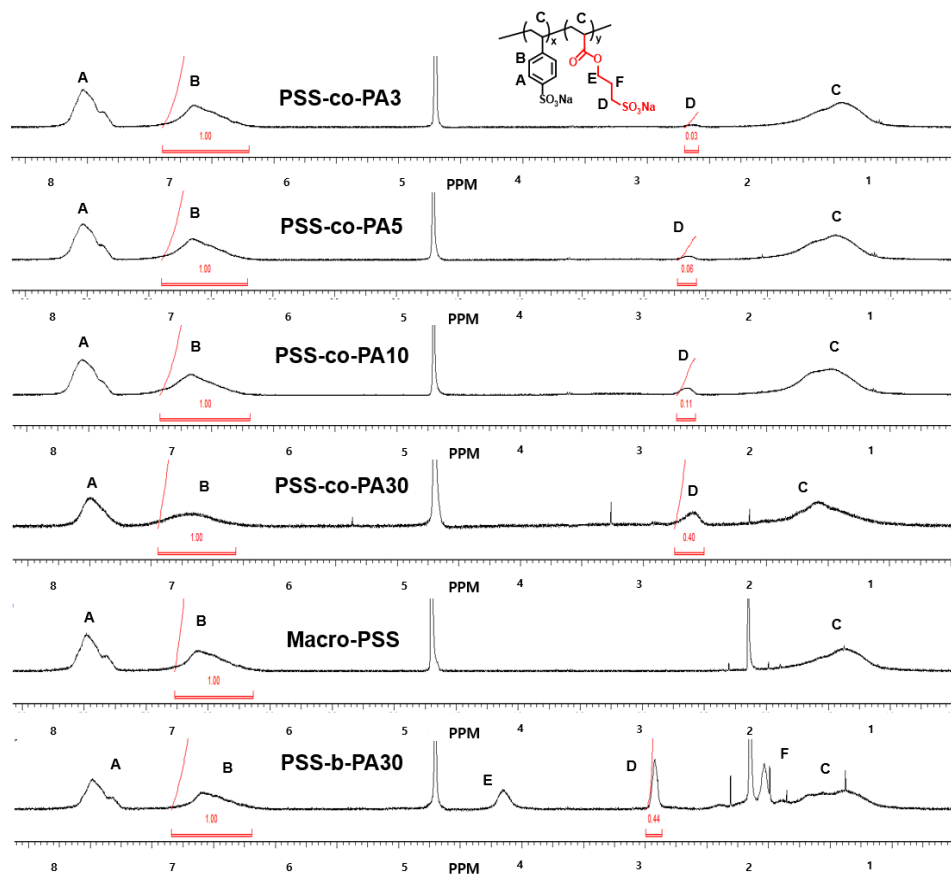


Figure 1. the ^1H NMR spectrum of PSS-PA series polymers.

Moreover, it can be seen from the FT-IR spectra of the copolymers shown in **Figure 2** that the vibrational bands are located between $1,640\text{ cm}^{-1}$ and $1,495$ to $1,412\text{ cm}^{-1}$ regarding the backbone vibrations of C=C in the aromatic ring. The vibrational band with a broad shoulder between $1,250$ and $1,140\text{ cm}^{-1}$ was attributed to the SO_3 asymmetric stretching vibration. Obviously, the peak of the ester stretching band at 1725 cm^{-1} appeared in the high contents of alkyl sulfonate groups in the PSS-PAs copolymers. The aqueous dispersions of PEDOT:PSS-PAs composites were obtained by oxidative polymerization using the EDOT monomer in PSS-PAs copolymers as templates. The FT-IR spectra of the PEDOT:PSS-PAs composites were presented in **Figure 2(b)**. The composites have the same C=C stretching band at 1624 cm^{-1} , the C-C stretching band at 1523 cm^{-1} and the C-O-C stretching band at 1388 cm^{-1} as the

spectrum of EDOT monomer. The results indicated that the synthesis of PEDOT:PSS-PAs composites was adequately prepared.

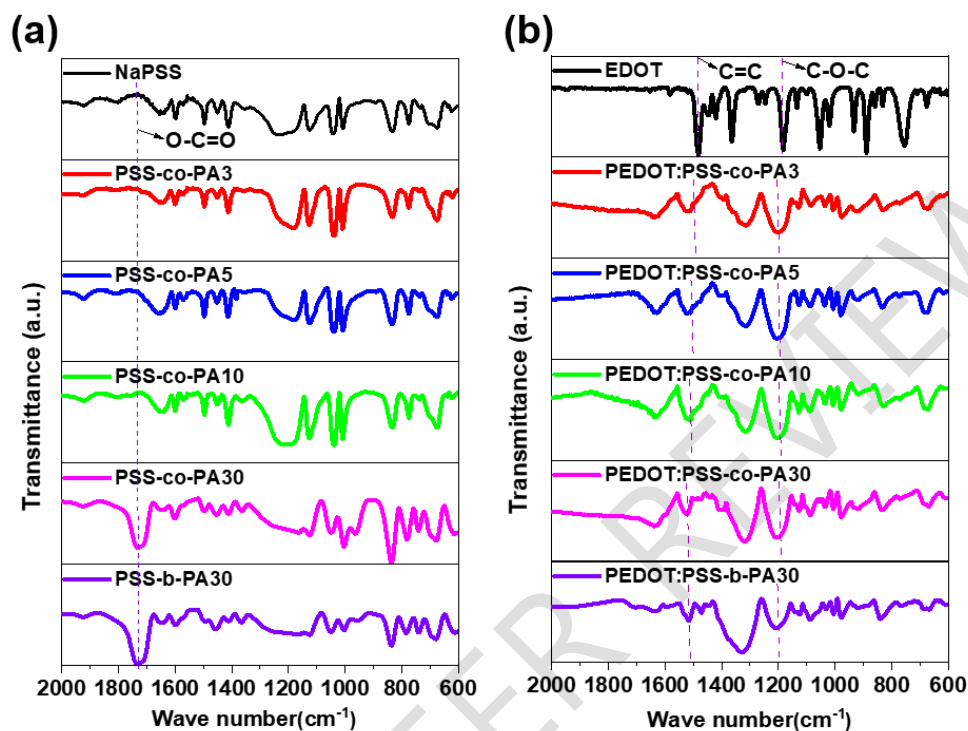


Figure 2. FT-IR spectra of NaPSS and PSS-PA series, and PEDOT:PSS series complexes.

The maximum solubility could be affected by the contents of alkyl sulfonate functional groups in the PSS-PA series polymers. The solubility was measured by preparing a saturated PSS-PA series solution in water. The mass of the PSS-PA series polymers was weighed after evaporation of the known volume of the saturated solutions. The solubility was 198, 336, and 376 mg/mL for the PSS, PSS-co-PA30, and PSS-b-PA30, respectively. This result might be due to the introduction of flexible alkyl sulfonate functional groups. The block copolymer (PSS-b-PA30) showed the better solubility compared to that of random copolymer (PSS-co-PA30).

UV-vis-NIR absorption spectra of PEDOT:PSS-PAs composites was exhibited shown in **Figure 3**. The absorbance behavior of the composites has been found to be very similar in all wavelength ranges, and it could be assumed that the PEDOT doping levels in the PSS-PAs copolymers were also similar.[17] This suggests that the incorporation of alkyl sulfonate groups into PSS polymers is rather independent of the degree of PEDOT doping.

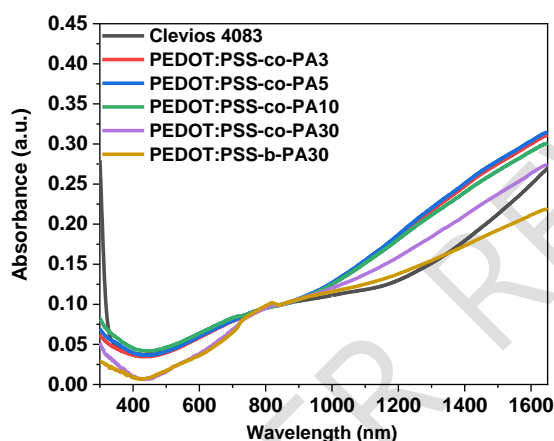


Figure 3. UV-vis absorption spectra of Clevios 4083 and PEDOT:PSS-PA series films.

The sheet resistance could be affected by the contents of alkyl sulfonate groups in the PEDOT:PSS-PAs composites. To obtain the films of Clevios 4083 and PEDOT:PSS-PAs composites, the solutions were spin-coated on cleaned glass substrates at 1500 rpm for 60s and the films were dried at 60°C in a vacuum oven for overnight. The sheet resistance of the composite films was measured with a four-point probe method. It exhibited 2.24, 1.2, 0.84, 0.75, 0.41, and 0.62 Mohm sq⁻¹ for the Clevios 4083, PEDOT:PSS-co-PA3, PEDOT:PSS-co-PA5, PEDOT:PSS-co-PA10, PEDOT:PSS-co-PA30 and PEDOT:PSS-b-PA30, respectively (**Figure 4**). It is worth noting that the sheet resistance has significant reduction compared to that of the Clevios 4083 film. These results might be explained by the increased molecular weight of PEDOT in the PSS-PA copolymer.

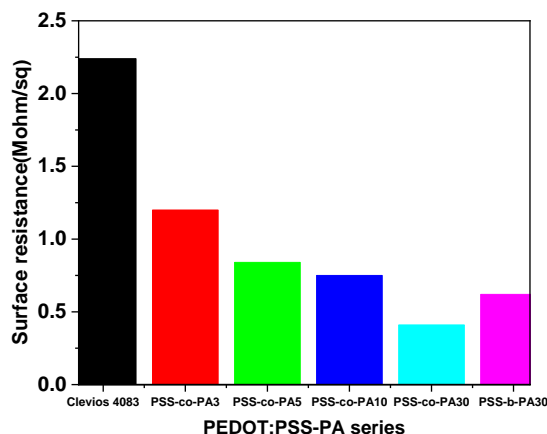


Figure 4. Sheet resistance of PEDOT: PSS and PEDOT:PSS-PA series films.

For investigating the effect of alkyl sulfonate contents on the PEDOT polymerization, XPS was used to quantify the ratio of PEDOT to PSS-PA copolymers. The findings of an analysis of the surface chemistry of the PEDOT:PSS and PEDOT:PSS-PA series powders are displayed in **Figure 5** and **Table 1**. **Figure 5(a, c)** displayed the deconvolution of the C (1s) spectrum of PEDOT:PSS-co-PA30 and PEDOT:PSS-b-PA30 composites for two different binding energy peaks at 284.8 and 286.4 eV, which correspond to C-C sp² and C-O. Moreover, we can observe the emergence of binding energy peaks at 288.4 eV, which correspond to O-C=O sp² for PEDOT:PSS-co-PA30 and PEDOT:PSS-b-PA30 powders. This is another indication that alkyl sulfonate groups have been successfully polymerized in the main chain of PSS-PAs. As shown in **Figure 5(b, d)**, the S(2p) spectrum found two peaks in PEDOT with low binding energy and in PSS-PAs with high binding energy due to their different chemical environments.[18] With three surrounding oxygen atoms, the S(2p) peak in PSS-PA with a high electronegativity environment is measured at a higher binding energy. Moreover, the S(2p) peak in PEDOT with lower electronegativity was measured at a lower binding energy. Then, the S(2p) spectrums of PEDOT:PSS-co-PA30 and PEDOT:PSS-b-

PA30 powders can be deconvoluted into four peaks at 168.0, 167.7, 164.6 and 163.5 eV. The lower binding energy peaks at 164.6 and 163.5 eV are relevant to the sulfur spin-orbital coupling ($S2p_{3/2}$) and ($S2p_{1/2}$) in PEDOT, whereas the higher binding energy peaks at 168.0 and 167.7 eV are derived from the sulfur spin-orbital coupling ($S2p_{3/2}$) and ($S2p_{1/2}$) in PSS-co-PA30 and PSS-b-PA30. Furthermore, the thiophene-sulfonate ratio ($R_{T/S}$) was used to denote the ratio of PEDOT to PSS-PA.[19] $R_{T/S}$ can be determined from the S($2p$) peak area ratio of PEDOT and PSS. The $R_{T/S}$ ratio of PEDOT: PSS-co-PA30 (~0.45) is more than two times higher than that of Clevios 4083 (~0.22), as shown in **Table 1**. Therefore, the polymerization of PEDOT with PSS-co-PA30 was superior to that of PSS. This also explains why the sheet resistance of PEDOT:PSS-co-PA30 is significantly lower than that of Clevios 4083. However, the $R_{T/S}$ of PEDOT:PSS-b-PA30, PEDOT:PSS-co-PA3, PEDOT:PSS-co-PA5 and PEDOT:PSS-co-PA10 composites decreased slightly compared to PEDOT:PSS-co-PA30, which also indicated that their sheet resistant was slightly increased. These results also demonstrate that the anionic group of the alkyl sulfonate also provides doping performance for the synthesis of PEDOT.

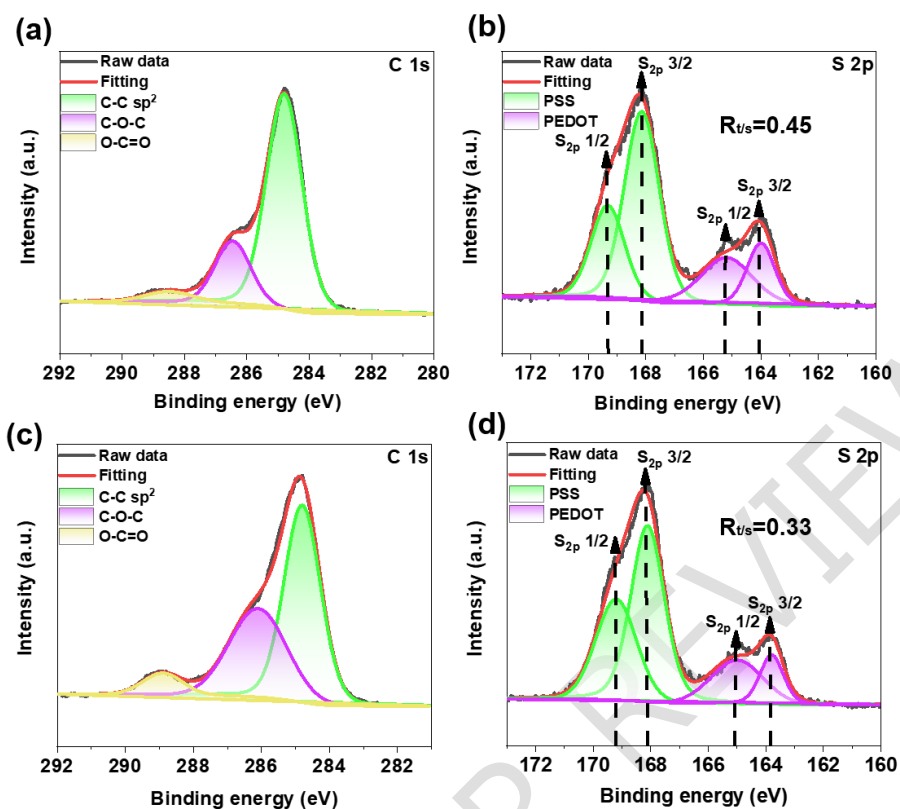


Figure 5. XPS spectra (a) C (1s), (b) S (2p) of PEDOT:PSS-co-PA30; (c) C (1s), (d) S (2p) of PEDOT:PSS-b-PA30.

Table 1. Atomic composition of Clevious 4083 and PEDOT: PSS-PA series with XPS-based analysis.

Samples	C (%)	O (%)	S (%)	$R_{T/S}$ ratio
Clevious 4083	65.15	23.57	8.61	0.22
PEDOT:PSS-co-PA3	63.49	27.64	8.88	0.32
PEDOT:PSS-co-PA5	63.62	27.96	8.42	0.30
PEDOT:PSS-co-PA10	60.84	30.5	8.66	0.31
PEDOT:PSS-co-PA30	61.99	28.78	9.23	0.45
PEDOT:PSS-b-PA30	59.16	31.78	9.06	0.33

In order to study the influence on morphology of the synthesized PEDOT:PSS-PAs films, the atom force microscope (AFM) was measured. Clevios 4083 and PEDOT:PSS-PA films were made using spin-coating method and annealed at 140°C for 30minutes. From **Figure 6**, we could observe the films were fabricated successfully and all composites had a good film-forming properties. The topographic image of the PEDOT:PSS-PAs films were very similar to that of Clevios 4083 film. In addition, the root mean square (RMS) values of composite films were below 20 nm. It displayed 6.3, 15.1, 16.5, 17.1, and 19.7 nm for the Clevios 4083, PEDOT:PSS-co-PA3, PEDOT:PSS-co-PA5, PEDOT:PSS-co-PA10, PEDOT:PSS-co-PA30, and PEDOT:PSS-b-PA30, respectively. The RMS values of PEDOT:PSS-PA films increased with the content of alkyl sulfonate groups. This demonstrated that the introduction of the alkyl sulfonate groups into the PSS polymers changed the conformation of PEDOT chains.

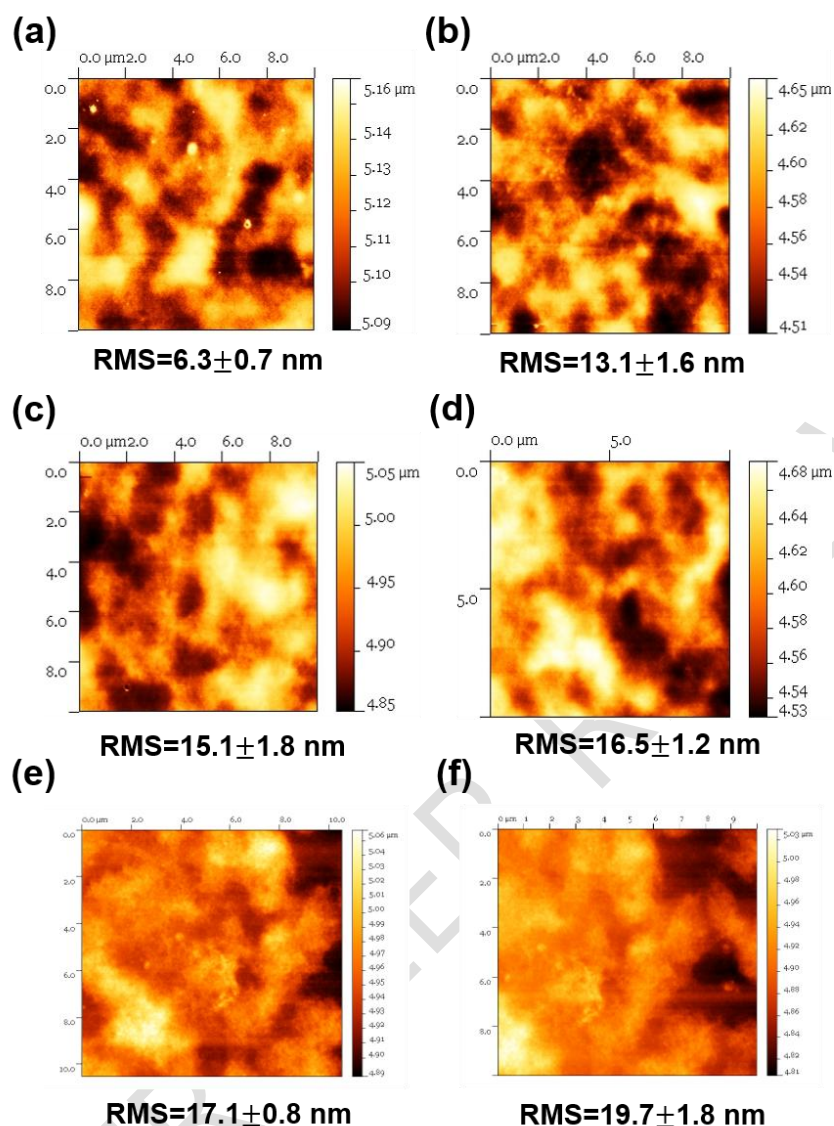
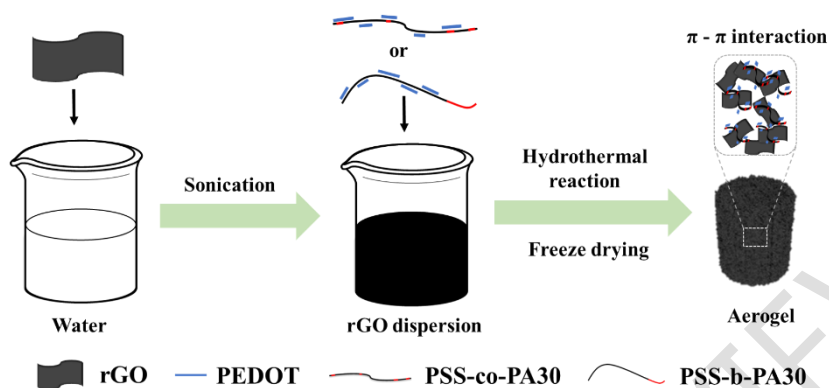


Figure 6. AFM topography images of Clevios 4083 (a), PEDOT: PSS-co-PA3 (b), PEDOT: PSS-co-PA5 (c), PEDOT: PSS-co-PA10 (d), PEDOT: PSS-co-PA30 (e), and PEDOT: PSS-b-PA30 (f) films;

All films were annealed at 140 ° C.

To study the electrochemical performance of PEDOT:PSS-co-PA30/rGO electrodes, the solution of Clevios 4083, and PEDOT:PSS-co-A30 composites were added to rGO dispersion with the ratio of 30:1 and mixed through sonication for 6 hours (**Scheme 2**). Then the

PEDOT:PSS-co-PA30/rGO aerogels was prepared through the hydrothermal reaction and freeze-drying process.



Scheme 2. Preparation of /PEDOT:PSS-co-PA/rGO composites.

As shown in **Figure 7**, the morphologies of the porous PEDOT:PSS-co-PA30/rGO and Clevios 4083/rGO aerogels was investigated using FESEM. All of the Clevios 4083/rGO, and PEDOT:PSS-co-PA30/rGO aerogels, displayed a 3D network structure formed by graphene sheets. Among them, the aerogel structure in Clevios 4083/rGO appeared to be relatively stacked and had a disordered distribution of pores. In the aerogel structure of PEDOT:PSS-co-PA30/rGO, a number of relatively large pores are observed. The elemental distributions of carbon (C), oxygen (O), and sulfur (S) were further investigated using EDX mapping for investigating the distribution of rGO and PEDOT:PSS-co-PA30 in PEDOT:PSS-co-PA30/rGO. As shown in **Figure 7(c, d)**, the S elements embedded only in PEDOT:PSS-co-PA30 are well distributed in the whole composite network, thus demonstrating the uniformity and continuity of the large scale distribution of PEDOT:PSS-co-PA30.

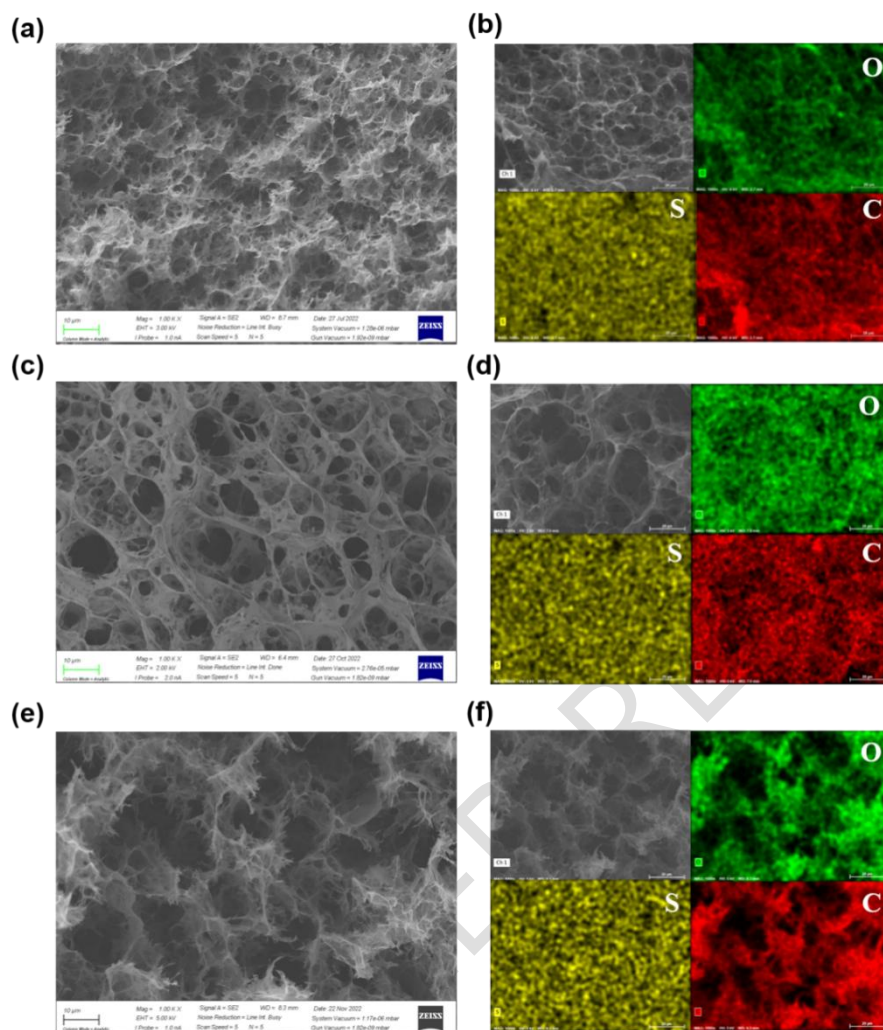


Figure 7. Low-magnification FESEM images of Clevios 4083/rGO aerogel (a); PEDOT:PSS-co-PA30/rGO aerogel (c); and PEDOT:PSS-co-PA30/rGO aerogel (e), SEM image and elemental mappings of C, O and S of PEDOT:PSS/rGO aerogel (b); PEDOT:PSS-co-PA30/rGO aerogel (d); PEDOT:PSS-co-PA30/rGO aerogel (e).

Figure 8(a) displayed electrochemical impedance spectroscopy (EIS) performed in the frequency range of 10 mHz to 10 kHz. The slope of the straight line in the low frequency region is due to the charge transfer behavior dominated by the reaction kinetics. The diameter of the semicircle is the resistance during charge transfer (R_{ct}). The R_{ct} values for Clevios

4083/rGO and PEDOT:PSS-co-PA30/rGO aerogel electrodes can be calculated to be 0.346, and 0.271 Ω , respectively. This indicated that PEDOT:PSS-co-PA30 had a more efficient connection with rGO in comparison to PEDOT:PSS and reduced their connection resistance. This might be due to the fact that PEDOT:PSS-co-PA30 has a higher molecular weight of PEDOT. **Figure 8 (b, c)** exhibited the CV curves of Clevios 4083/rGO and PEDOT:PSS-co-PA30/rGO aerogel electrodes at the scan rate of 5 mV S^{-1} . The two aerogels showed a rectangular-like shape and appeared as redox peaks. In addition, the specific capacitances of the Clevios 4083/rGO and PEDOT:PSS-co-PA30/rGO aerogel electrodes was determined using CV curves at the different scan rates ranging from 5 to 300 mV S^{-1} . The highest specific capacitance of PEDOT:PSS-co-PA30/rGO (103.4 F g^{-1}) at 5 mV S^{-1} is slightly decreased compared to that of Clevios 4083/rGO. However, PEDOT:PSS-co-PA30/rGO aerogel electrodes shows a better speed capacity with 44% capacity retention when the scan speed is increased from 5 to 300 mV S^{-1} compared to that of Clevios 4083/rGO. The cycle stability of the Clevios 4083/rGO and PEDOT:PSS-co-PA30/rGO aerogel electrodes was measured at the current density of 0.3 A/g in **Figure 8(d)**. The rGO/PEDOT:PSS-co-PA30 electrode retained 88% of its initial capacitance after 5000 cycles. Thus, the rGO/PEDOT:PSS-co-PA30 electrode exhibited excellent stability in comparison to that of Clevios 4083/rGO.

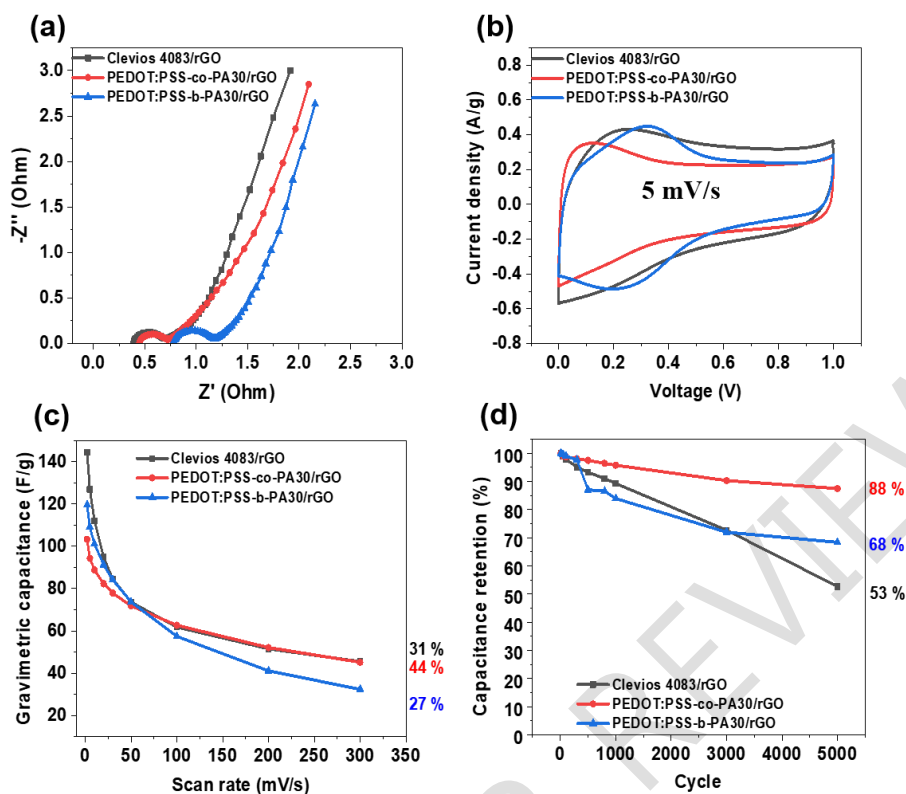


Figure 8. Electrochemical performances of the Clevios 4083/rGO, PEDOT:PSS-co-PA30/rGO and PEDOT:PSS-b-PA30/rGO aerogels. Nyquist plots (a); CV curves at the scan rate of 5 mV s^{-1} (b); Specific capacitances with scan rates ranging from 5 to 300 mV s^{-1} (c); Cyclic stability at the scan rate of 100 mV s^{-1} (d).

Conclusion

We successfully synthesized PEDOT: PSS-co-PA series by using PSS-co-PA series copolymers as the dopants. The content of alkyl sulfonate functional groups in the PSS-co-PA backbone can be confirmed by NMR and FT-IR spectra. The XPS data showed that the growth of PEDOT was enhanced by the introduction of alkyl sulfonate functional groups into PSS. Hence, PEDOT: PSS-co-PA30 had a significant reduced in sheet resistance compared to that of commercially available Clevios 4083 without any solvent treatment. Furthermore, the cycle stability using PEDOT: PSS-co-PA30/rGO electrode (88%) was improved compared to

that of Clevios 4083/rGO electrode (53%) after 5000 cycles. Therefore, we can expect these findings to promote the development of other optoelectronic devices.

Reference:

- [1] D. Liu, L. C. Chen, T. J. Liu, T. Fan, E. Y. Tsou, C. Tiu, *Adv. Chem. Engineer. Sci.*, 2014, **4**, 515.
- [2] W. Martin, R. J. Brodd, *Chem. Rev.*, 2004, **104**, 4245.
- [3] J. R. Miller, P. Simon, *Science.*, 2008, **321**, 651.
- [4] X. Lang, A. Hirata, T. Fujita, M. Chen, *Nat. Nanotechnol.*, 2011, **6**, 232.
- [5] G. Wang, L. Zhang, J. Zhang, *Chem. Soc. Rev.*, 2012, **41**, 797.
- [6] X. Gao, L. Zu, X. Cai, C. Li, H. Lian, Y. Liu, X. Wang, X. Cui, *Nanomaterials*. 2018, **8**, 335.
- [7] D. Villers, D. Jobin, C. Soucy, D. Cossement, R. Chahine, L. Breau, D. Bélanger, *J. Electrochem. Soc.*, 2003, **150**, A747.
- [8] S. A. Hashmi, H. M. Upadhyaya, *Solid State Ion.*, 2002, **152**, 883.
- [9] H. E. Yin, C. F. Lee, W.Y. Chiu, *Polymer.*, 2011, **52**, 5065.
- [10] C. Peng, G. A. Snook, D. J. Fray, M. S. P. Shaffer, G. Z. Chen, *Chem. Commun.*, 2006, **44**, 4629.
- [11] H. Randriamahazaka, C. Plesse, D. Teyssie, C. Chevrot, *Electrochem. Commun.*, 2004, **6**, 299.
- [12] A. M. White, R. C. T. Slade, *Electrochim. Acta.*, 2004, **49**, 861.

[13] Z. Hu, J. Zhang, Z. Hao, Y. Zhao, *Sol. Energy Mater. Sol. Cells.*, 2011, **95**, 2763.

[14] W. Cai, X. Ma, J. Guo, X. Peng, S. Zhang, Z. Qiu, J. Ying, J. Wang, *J. Appl. Polym. Sci.*, 2017, **134**, 45163.

[15] H. Yano, K. Kudo, K. Marumo, H. Okuzaki. *Sci. Adv.*, 2019, **5**, 9492.

[16] K. H. Hwang, H. J. Seo, S. H. Nam, J. H. Boo, *Nanosci. Nanotechnol.* 2015, **15**, 10.

[17] H. W. Heuer, R. Wehrmann, S. Kirchmeyer, *Adv. Funct. Mater.*, 2002, **12**, 89.

[18] L. Li, X. Li, Y. Shen, X. Chen, L. Jiang, *e-Polymers.*, 2021, **21**, 779.

[19] N. Y. Park, G. S. Jeong, Y. J. Yu, Y. C. Jung, J. H. Lee, J. H. Seo, J. Y. Choi, *Polymers.*, 2022, **14**, 478.

UNDER PEER REVIEW